metals

MDPI

Article

Transformations of the Microstructure and Phase Compositions of Titanium Alloys during Ultrasonic Impact Treatment. Part I. Commercially Pure Titanium

Alexey Panin [1,*], Andrey Dmitriev [1], Anton Nikonov [1], Marina Kazachenok [1], Olga Perevalova [1] and Elena Sklyarova [2]

[1] Institute of Strength Physics and Materials Science of Siberian Branch of Russian Academy of Sciences, 634055 Tomsk, Russia; dmitr@ispms.ru (A.D.); anickonoff@ispms.ru (A.N.); kms@ispms.tsc.ru (M.K.); perevalova52@mail.ru (O.P.)

[2] National Research Tomsk Polytechnic University, 634050 Tomsk, Russia; skea@tpu.ru

* Correspondence: pav@ispms.tsc.ru; Tel.: +7-3822-286-979

Abstract: Experimental and theoretical studies helped to reveal patterns of surface roughening and the microstructure refinement in the surface layer of commercial pure titanium during ultrasonic impact treatment. Applying transmission electron microscopy technique, a gradient microstructure in the surface layer of the ultrasonically treated sample, where the grain size is varied from nano- to micrometers was revealed. It was shown that the surface plastic strains of the titanium sample proceeded according to the plastic ploughing mechanism, which was accompanied by dislocation sliding, twinning, and the transformations of the microstructure and phase composition. The molecular dynamics method was applied to demonstrate the mechanism of the phase transformations associated with the formation of stacking faults, as well as the reversible displacement of atoms from their sites in the hcp lattice, causing a change in coordination numbers. The role of the electronic subsystem in the development of the strain-induced phase transformations during ultrasonic impact treatment was discussed.

Keywords: titanium; phase transformation; electronic structure; microstructure; molecular dynamics; ultrasonic impact treatment; transmission electron microscopy

Citation: Panin, A.; Dmitriev, A.; Nikonov, A.; Kazachenok, M.; Perevalova, O.; Sklyarova, E. Transformations of the Microstructure and Phase Compositions of Titanium Alloys during Ultrasonic Impact Treatment. Part I. Commercially Pure Titanium. *Metals* **2021**, *11*, 562. https://doi.org/10.3390/met11040562

Academic Editor: Francesca Borgioli

Received: 15 March 2021
Accepted: 26 March 2021
Published: 30 March 2021

1. Introduction

Ultrasonic impact treatment (UIT) is an effective method of surface hardening that significantly improves the functional properties of structural materials, as well as their welded joints [1]. Surface processing with a high-strength striker vibrating at an ultrasonic frequency results in a notable change in the microstructure of metals and alloys due to the refining of existent grains and the formation of new ones. Also, it enhances the density of dislocations and curvature of slip planes, promotes the transformation of the martensitic microstructure, the partial decomposition of supersaturated solid solutions, and the precipitation of second phase particles, as well as raises elastic micro- and macro-stresses, etc. As a result, the surface layer microhardness of the structural materials is increased, and the strength, wear, creep, and corrosion resistance (in addition to other characteristics) are improved [2–5]. Generally, the nature of morphological changes taken place in the materials during the UIT processing is determined not only by the temperature–rate parameters, but also by their microstructures, phase compositions, the presence of carbide-forming elements, possible polymorphic transformations under severe plastic strains, etc.

As a rule, the microstructure evolution in the structural materials during the UIT processing is discussed within the framework of a one-level approach based on the theory of dislocations. In particular, it has been shown that strains of the surface layer of

titanium and its alloys (which are widely used in the aerospace, nuclear and other industries) are developed according to the plastic ploughing mechanism during repeated penetrations of a striker into the treated specimen [6–8]. In this case, intense sliding and twinning of dislocations take place, causing the formation of sub-grains with low-angle misorientations, as well as their subsequent transformation into nanocrystalline grains with high-angle misorientations.

According to [9,10], under conditions of strong deviations from equilibrium, self-organized processes with the formation of new space-dissipative structures take place, which provide significant changes in the initial mechanical properties of materials. It has been convincingly shown in the papers of V.E. Panin [11,12] that the nucleation and propagation of all strain defects in a loaded crystal (regardless of their dimension) is based on the development of local transformations of the microstructure and phase composition controlled by the electronic subsystem of the crystal. In the space of interstices of the crystal lattice characterized by a high degree of distortion, new (possible) microstructural states can be formed, which ensure the development of diffusionless shear strains of the crystal under external applied stresses. In doing so, computer simulation is an effective tool for studying atomic mechanisms underlying structural and phase transformations in a loaded solid. Earlier, the authors of the article, using the molecular dynamics method, demonstrated the development of $\beta \rightarrow \alpha \rightarrow \beta$ phase transformations in the Ti-6Al-4V titanium alloy during scratch testing, which made it possible to explain the experimentally observed recovery of a scratch [13].

This paper opens a new series devoted to the study of transformations of the microstructure and phase compositions of titanium alloys during the UIT processing. In particular, the roles of dislocation slips, twinning, and phase transformations in refining the microstructure in the surface layer of commercially pure titanium (CP-Ti) are considered experimentally and using molecular dynamic simulation. The CP-Ti is used as a model material, in which the effect of alloying elements (aluminum, vanadium, etc.) on the instability of the crystal lattice of the α phase solid solution is not taken into account.

2. Materials and Methods

The as-received CP-Ti (the VT1-0 according to the Russian classification) was investigated with the following chemical composition (wt.%): 0.2 Al, 0.4 Zr, 0.3 Mn, 0.01 Cr, 0.06 Si, 0.2 Fe, 0.02 Cu, and 98.8 Ti. The average grain size was 70 μm.

The UIT processing of a plate 50 mm × 50 mm × 1 mm in size was carried out using a spherical striker 10 mm in diameter, fabricated from the hard alloy with composition WC-8 wt.% Co. During the UIT processing, the striker vibrated at a frequency of ~22 kHz and an amplitude of ~40 μm. Its movement speed was 0.2 m/s and load was 200 N.

After the UIT processing, the surface morphology of the sample was examined using a NewView 6200 optical profilometer (Zygo Corp., Middlefield, CT, USA) and a Solver HV atomic force microscope (NT-MDT, Moscow, Russia). A microstructural analysis was performed using a JEM 2100 (JEOL, Akishima, Tokyo, Japan) transmission electron microscope (TEM) with an electron acceleration energy of 200 kV. The cross-sectional TEM samples were manufactured, using a JEOL Ion Slicer EM-091001S (JEOL, Akishima, Tokyo, Japan). During preparation, argon was used as the working gas, the accelerating voltage was 8 kV, and the etching angle was 1.5 to 4°.

Microhardness was measured using a 'PMT-3' hardness tester (LOMO, St. Petersburg, Russia) with a load on the diamond pyramid of 50 g.

The dislocation density p was determined by the rectangular grid method using the following expression:

$$p = (n_1/l_1 + n_2/l_2) \cdot M/t, \quad (1)$$

where n_1 and n_2 were the numbers of intersections; l_1 and l_2 were line lengths; M was magnification; t was the foil thickness.

A computer simulation of the UIT processing was carried out using the LAMMPS software package [14]. On the atomic scale, the simulation of the process was carried

out by successive triple indentations of a spherical indenter into an initially defect-free titanium crystallite in the form of a parallelepiped. The indenter was a sphere with a radius of 6.5 nm. The load was directed from the indenter center to atoms within this sphere. The load value was calculated by the $F = -k(R-r)^2$ ratio, where k was the indenter stiffness coefficient; R was the sphere radius; r was distance between the centers of the indenter and atoms [15]. The indenter was moved along the Z axis at a fixed depth of 3.5 nm with a constant indentation rate of 15 m/s. The indentation depth was chosen so that the maximum load on the indenter did not exceed 12 GPa. The crystallographic orientation of grains in the model crystallite was chosen as follows: the X, Y, and Z axes coincided with the $[2\bar{1}\bar{1}0]$, $[01\bar{1}0]$, and [0001] directions, respectively. The equilibrium atomic configuration of the model crystallite was determined by the minimum potential energy calculation. The interaction between atoms was described by the potential [16] assessed within the framework of the embedded atom method. The simulated system was considered as an NVE ensemble, in which the number of atoms, energy and volume were conserved. The movement equations were integrated using the high-speed Verlet algorithm with a time step of 0.001 ps. The total number of atoms exceeded 4.1 million. The Common Neighbor Analysis (CNA) and Dislocation Extraction Algorithm (DXA) of the OVITO software [17] were used to identify the crystal lattice defects produced by multiple indentations of the spherical indenter. The simulation of strains of the model crystallite was carried out considering the nucleation and movement of dislocations along certain crystallographic planes.

3. Experimental Research Results of Changes in the Surface Morphology and the Microstructure of the CP-Ti Sample during the UIT Processing

3.1. Patterns of the Surface Layer Roughening

The penetration of the spherical striker, vibrated at the ultrasonic frequency, into the CP-Ti surface layer was accompanied by extrusion of the material along its perimeter. Since the plate movement was relative to the vibrated striker during the UIT processing, pile-ups of the displaced titanium were strained and re-strained again along the striker perimeter at each subsequent impact [8]. At the ultrasonic frequency of 22 kHz and the movement speed of ~0.2 m/s, the distance between the centers of impact spots was ~10 μm. Since the impact spots were much larger (about 500 μm in diameter), most of the material was plastically displaced at the front of the moved striker at each subsequent impact. Small semicircular pile-ups remained behind the moved striker (Figure 1a,b), the distance between which corresponded to that between the centers of the impact spots, and their height reached 1 μm. In general, dimensions of the pile-ups and the distances between them were determined by the UIT processing parameters and the CP-Ti mechanical properties.

According to detailed studies performed using atomic force microscopy, the micro-roughness on the striker surface also caused local plastic ploughing of the processed material, which resulted in roughening of the semicircular pile-up surfaces due to the formation of numerous protrusions and depressions of various shapes and heights (Figure 1c,d).

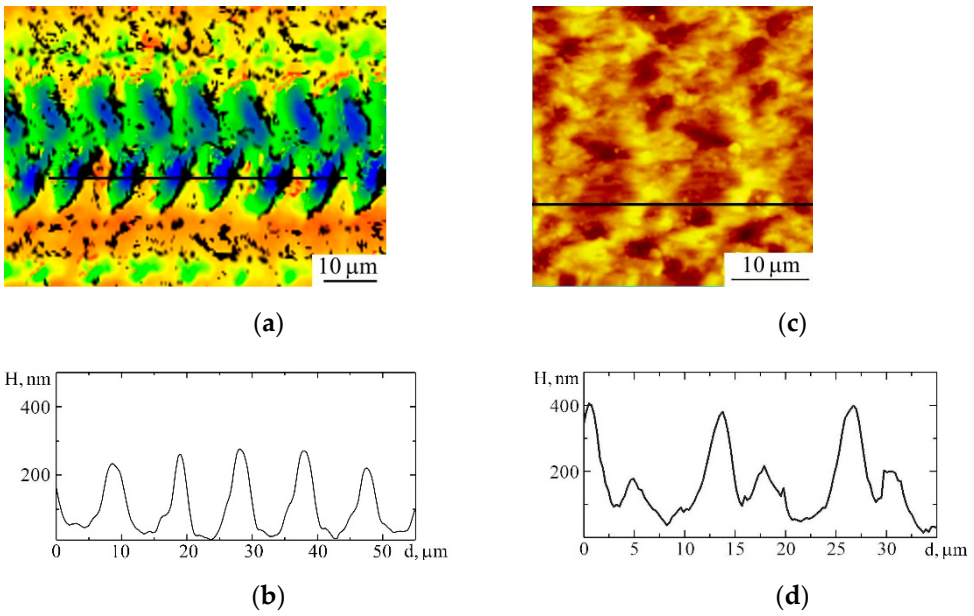

Figure 1. The surface morphology (**a**,**c**) and corresponding profilograms (**b**,**d**) of the CP-Ti sample after the ultrasonic impact treatment (UIT) processing. Optical profilometry (**a**,**b**) and atomic force microscopy (**c**,**d**).

3.2. TEM Studies of the Gradient Microstructure in the Surface Layer

TEM cross-sectional analysis of CP-Ti samples after the UIT processing revealed the gradient microstructure of their surface layers. Inside the uppermost surface layer, a sub-microcrystalline structure of the α phase with grain sizes of less than 200 nm was observed (Figure 2). High-angle misorientations of the α-Ti phase equiaxed grains were confirmed by the quasi-ring structure of an electron diffraction pattern (Figure 2c). The microstructure with a dislocation density of 10^{16} m^{-2} was found inside the α phase grains (Figures 3a and 4a). The bend contours in the TEM images are indicative of high residual stresses developing inside the layer under consideration.

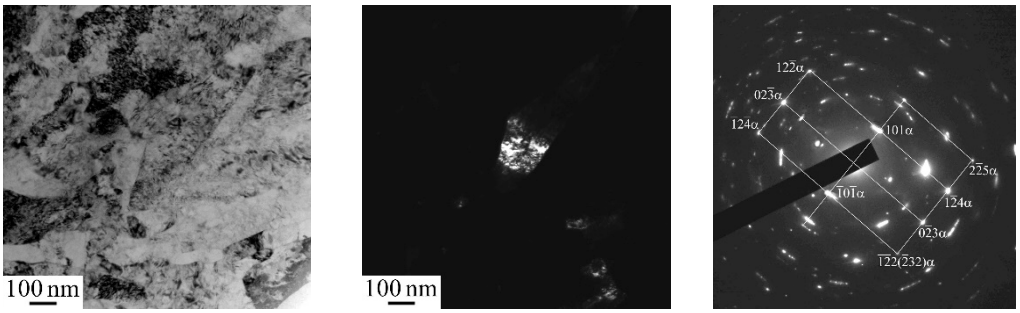

Figure 2. TEM bright- (**a**) and dark-field (**b**) images and associated selected area electron diffraction (SAED) patterns (**c**) of the microstructure of the uppermost surface layer of the CP-Ti sample after the UIT processing. TEM dark-field images were obtained with the $101\,(\bar{2}32)_{\alpha\text{-Ti}}$ reflection.

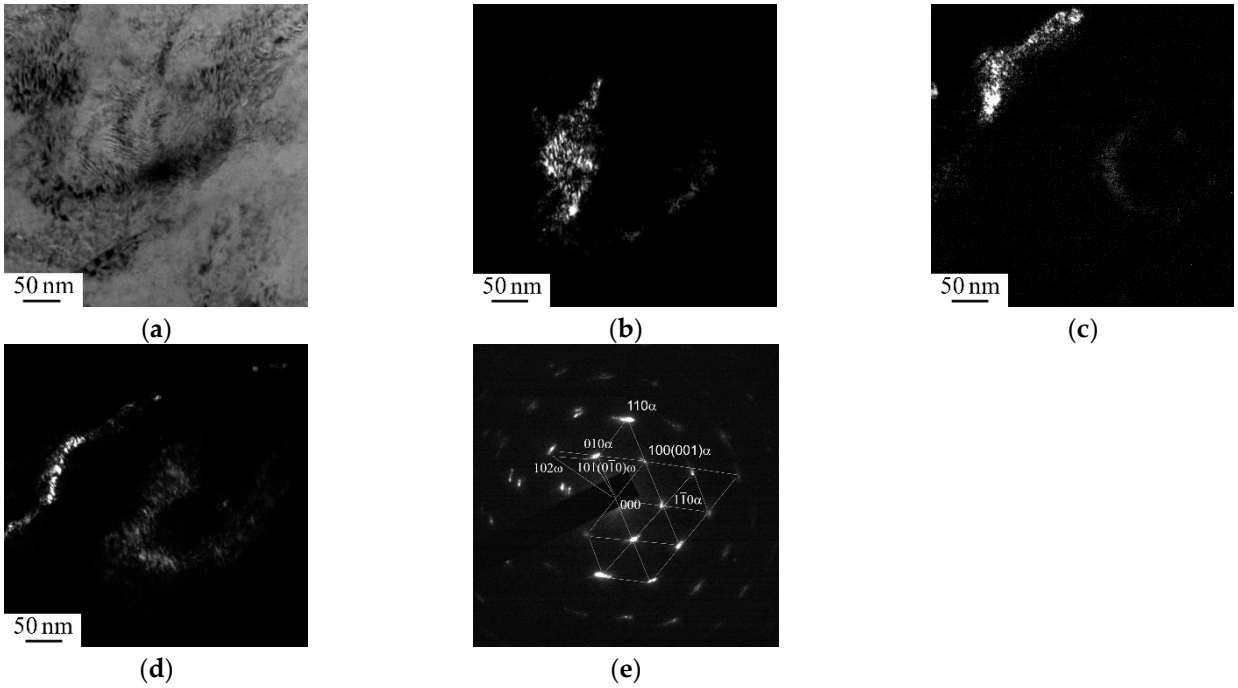

Figure 3. TEM bright- (**a**) and dark-field (**b**–**d**) images and associated SAED pattern (**e**) of the microstructure of the uppermost surface layer of the CP-Ti sample after the UIT processing. The dark-field images were obtained with the $110(001)_{\alpha\text{-Ti}}$ reflection (**b**), the closely spaced 120 $(001)_{\alpha\text{-Ti}}$ and 102 $\left(0\bar{1}0\right)_{\omega\text{-Ti}}$ ones (**c**), as well as in the 101 $\left(0\bar{1}0\right)_{\omega\text{-Ti}}$ reflex (**d**).

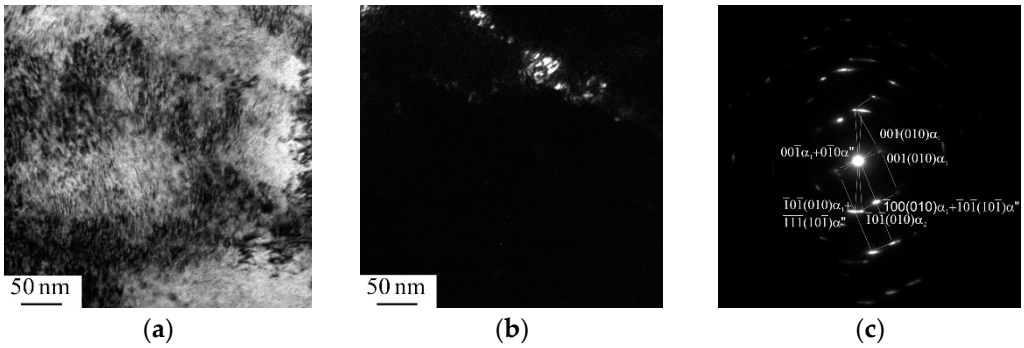

Figure 4. TEM bright- (**a**) and dark-field (**b**) images and associated selected area electron diffraction (SAED) pattern (**c**) of the microstructure of the uppermost surface layer of the CP-Ti sample after the UIT processing. TEM dark-field image was obtained with the $0\bar{1}0\left(10\bar{1}\right)_{\alpha''\text{-Ti}}$ reflection.

In addition to a refinement of the α phase grains, a significant change in the phase composition was observed in the uppermost surface layer of the CP-Ti sample after the UIT processing. It was due to the high chemical activity of titanium and its polymorphism (the ability to form various crystal microstructures). The ω and α″ phase crystallites with an average transverse size of 10 nm were found in grains and fragments of the α phase bounded by adjacent shear bands (Figures 3 and 4, respectively).

The α phase grains with an average size of 10 μm were observed in the surface layer 10 μm thick, inside which the banded microstructure and microtwins with an average transverse size of 100 nm were revealed (Figure 5a). It should be noted the presence of a large number of extinction contours indicated high internal stresses and distortions of the crystal lattice in the surface layer of the CP-Ti sample after the UIT processing. The dislocation density did not exceed 10^{14} m^{-2}.

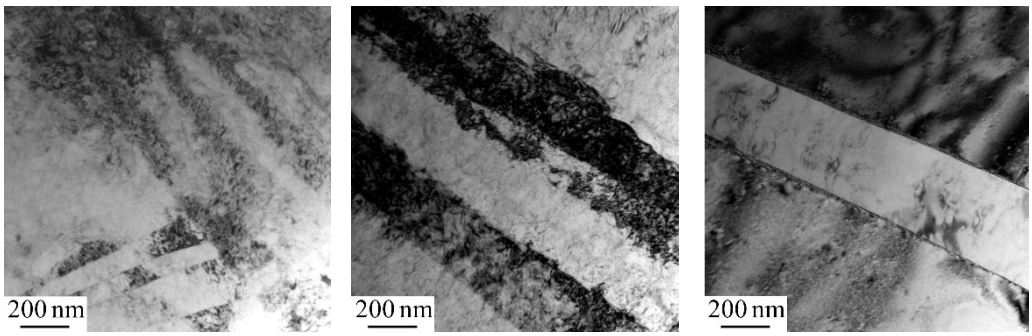

Figure 5. TEM bright-field images of the microstructure of the CP-Ti sample after the UIT processing, TEM images were obtained at depths of 10 (**a**) and 50 (**b**,**c**) μm below the surface of the sample.

At a depth of 50 μm, the average size of the α phase grains corresponded to that for the as-received CP-Ti. The transverse dimensions of the fragments separated by adjacent shear bands increased up to 300 nm. In addition, the boundaries of the banded substructures were strongly curved (Figure 5b). A large number of extinction contours were observed inside the fragments. In this case, the dislocation density did not exceed 5×10^{13} m^{-2}. Also, twins with an average transverse size of 300 nm were inside the α phase grains observed at this depth (Figure 5c) [18]. Finally, at a depth of 70–100 μm, the microstructure consisted of equiaxed α phase grains, in which dislocations were identical to the as-received CP-Ti.

The gradient microstructure of the surface layer of CP-Ti samples after the UIT processing makes itself evident in the microhardness variation across the sample. The uppermost surface layer of the samples exhibits the highest microhardness (2.2 GPa). As the depth below the sample surface increases, the microhardness gradually decreases down to a value characteristic of the base metal (1.6 GPa) at a depth of ~100 μm [18].

4. Molecular Dynamics Simulation of Strains of the Surface Layer of the Titanium Crystallite during the UIT Processing

Molecular dynamics simulation enabled a clear demonstration of the patterns of the surface layer roughening on the CP-Ti sample and the development of the microstructural transformations under repeated penetrations of the spherical striker. According to Figure 6, a pile-up of the strained material was crumpled and re-pushed back along its perimeter with each subsequent penetration of the indenter. In this case, small semicircular pile-ups were formed behind the moved indenter. The distance between them, as shown above, corresponded to that between the centers of the impact spots.

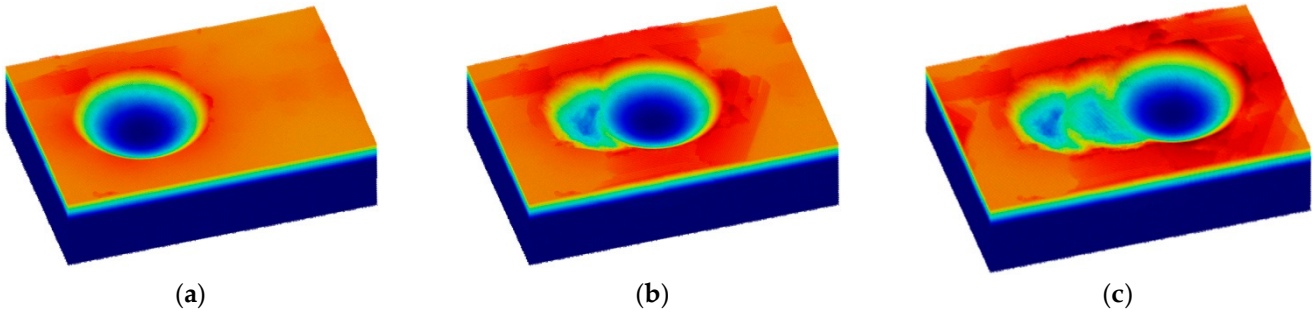

Figure 6. 3D images of the titanium crystallite after one (**a**), two (**b**) and three (**c**) penetrations of the spherical indenter.

The indenter penetration into the titanium crystallite was accompanied by the nucleation of dislocations in the area of its contact with the sample surface and their translational movement in easy-sliding directions, as well as the formation of twins (Figure 7a). The density of dislocations and twins increased continuously during its subsequent penetration

in the sample, causing fragmentation and reorientation of the crystal lattice (Figure 7b,c). In this case, the crystal lattice of the surface layer at the contact spot, as well as at the boundaries between twins and between misoriented fragments, was not identified as a regular atomic structure by the OVITO software due to the fact that some atoms had been displaced from their sites. Inside the fragments, local fcc regions (represented stacking faults) had been formed. However, other areas with the bcc lattice were at the boundaries of the fragments (Figure 8).

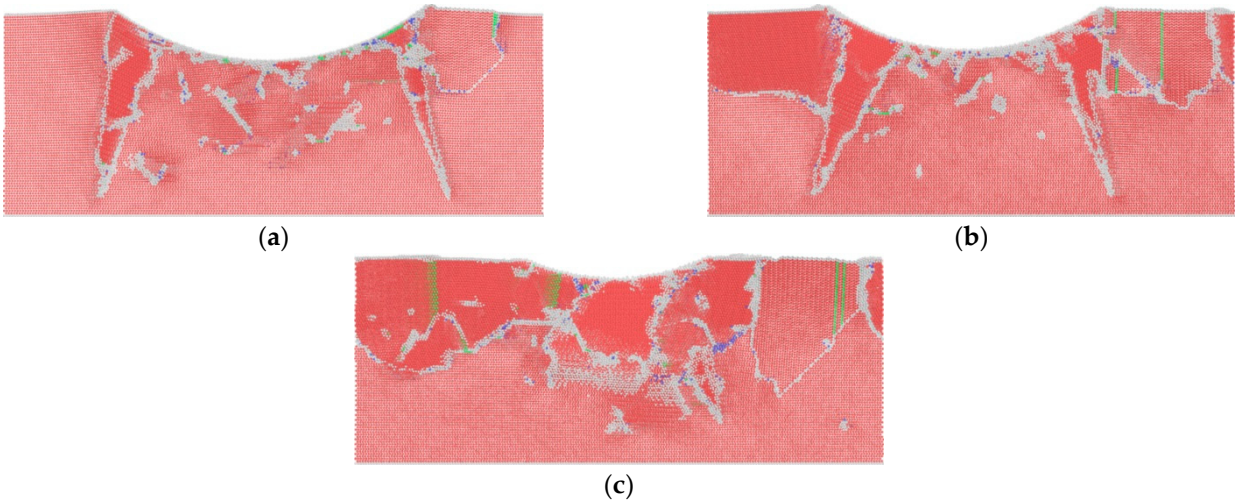

Figure 7. The microstructure of a layer of the titanium crystallite in the *YZ* plane 2 nm thick with *X* coordinates of 31 (**a**), 47 (**b**), and 63 nm (**c**) after the first (**a**), second (**b**) and third (**c**) penetrations of the indenter. Atoms that had formed the crystal lattice, in which some of them were displaced from their sites, are marked in light gray.

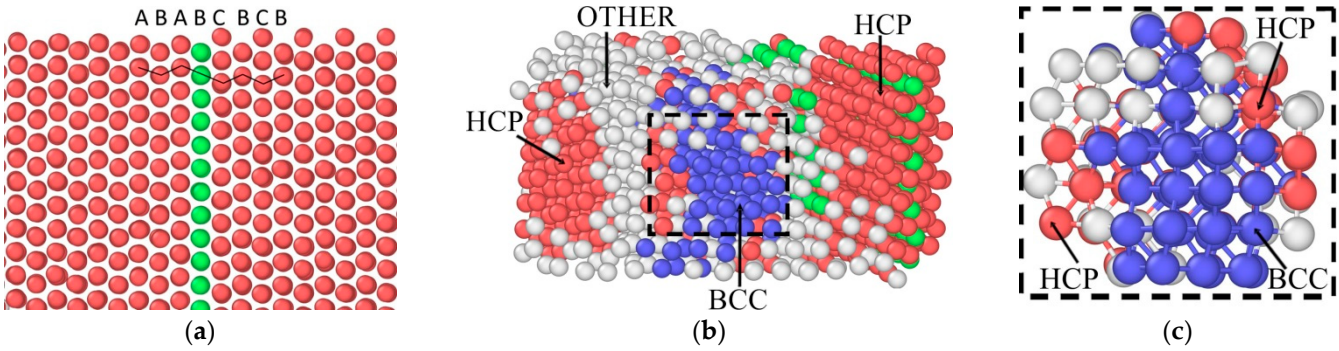

Figure 8. The formation of a stacking fault (**a**) and a local region with the bcc crystal lattice (**b**) in the titanium crystallite after three penetrations of the indenter. The color of atoms corresponds to different local configurations of the atomic lattice: blue is bcc, green is fcc, red is hcp, gray is an unidentified microstructure. Figure (**c**) corresponds to the central region fragment in (**b**) marked by a dotted line, depicting bonds between nearest atoms.

Figure 9 shows a local region with an unidentified crystal lattice (gray). It could be concluded from the analysis that the displacement of atoms from their sites in the hcp lattice was accompanied by a change in their coordination numbers (the number of nearest neighbors), which was an indirect evidence of the microstructure transformation in this defect area.

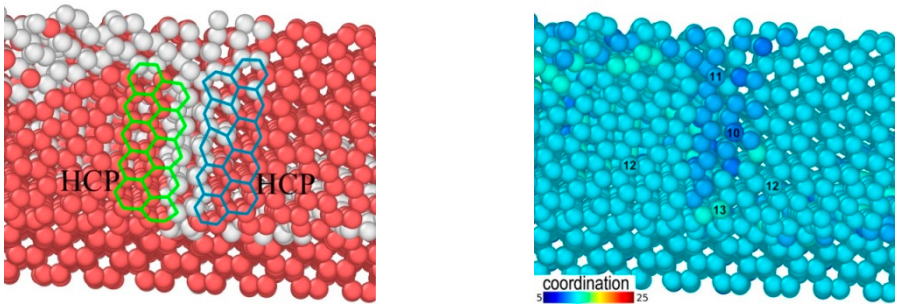

(**a**) (**b**)

Figure 9. The spatial arrangement of atoms (**a**) and their coordination numbers (**b**) in the defect region of the titanium crystallite after three penetrations of the indenter.

During repeated penetrations of the indenter into the initially defect-free titanium crystallite, a nonlinear increase in the number of atoms took place, which had a coordination number different from 12. As shown in Figure 10, the number of atoms belonged to the hcp structure gradually decreased that was visualized by computer simulation of the process. However, the number of such atoms slightly increased again at moments when the effect of an impact ceased and the next one began (0.4 and 0.8 ns).

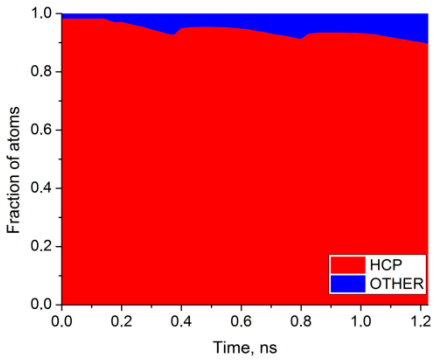

Figure 10. The time dependence of the number of atoms forming the hcp structure (red) and ones whose crystal lattice is different (blue).

5. Discussion

An impact of the spherical WC-Co striker on the CP-Ti sample surface, when only the normal compressive load was applied, could be described in the framework of the typical Hertz problem on the contact of a ball with an elastic half-space. The solution of the Hertz problem enabled the estimation of the contact spot radius a and the striker penetration depth δ using the following expressions [19]:

$$\left(\frac{3F_nR}{4E^*}\right)^{1/3}, \quad (2)$$

$$\delta = a^2/2R' \quad (3)$$

where F_n was the normal compressive load; $E^* = \left(\frac{1-v_1^2}{E_1} + \frac{1-v_2^2}{E_2}\right)^{-1}$ was the reduced Young's modulus of the striker–sample system (E_1, E_2 and ν_1, ν_2 were the Young's modulus and Poisson's ratio values of the striker and the CP-Ti sample, respectively); R was the curvature radius of the spherical striker.

The reduced Young's modulus of the "WC-Co-CP-Ti" system was 104 GPa. Accordingly, the striker 10 mm in diameter penetrated in the CP-Ti sample to a depth of 3.6 μm with the formation of a pile-up of displaced material along the contact spot perimeter at the

initial moment (when the magnetostrictor was turned off and the load was 200 N). In this case, the contact spot radius was 190 μm. During the UIT processing, the magnetostrictor elongation was 20 μm, and, therefore, the striker penetrated the surface layer of the sample to a great depth. Since the contact spot radius observed in the experiment was 500 μm, the penetration depth reached 6.25 μm according to Expression (3). It worth noting that the mathematical model of a cyclic random process [20] can be successfully applied to quantitative estimate the parameters of morphological structures.

As shown by molecular dynamics simulation, the spherical indenter penetration into the titanium crystallite was accompanied by intense dislocation slipping, which caused the crystallite fragmentation into sub-grains with the low-angle misorientation and twinning. During the repeated indenter penetrations, the lengths of the low-angle boundaries gradually increased, and the grain and sub-grain microstructure was formed in the surface layer of the titanium sample. Combined with high compressive residual stresses, this hindered the movement of dislocations into the bulk material along easy-slip planes. As a result, the plastic strain zone gradually narrowed around the indenter. In addition, the material transfer from the contact spot to the free surface was significantly enhanced, causing the formation of pile-ups. According to experimental data, the surface layer thickness, in which dislocation slipping and twinning had been developed during the UIT processing, did not exceed 100 μm. At the same time, the CP-Ti phases had been also transformed in the uppermost surface material due to strains by the plastic ploughing mechanism. This fact was confirmed by the observed ω and α″ nanocrystalline phases.

According to the results of molecular dynamics simulation, the phase transformations developed even after triple indenter penetrations into the titanium crystallite. This was associated with the formation of both stacking faults and local regions with a disordered arrangement of atoms at the boundaries between misoriented fragments of the hcp lattice. In particular, the formation of a stacking fault caused by the movement of a partial dislocation resulted in the appearance of several layers with the three-layer packing (the fcc microstructure) in the hcp titanium crystallite (two-layer packing) [21]. In turn, clusters with the bcc lattice could be formed at the boundaries between the misoriented hcp fragments. It could be assumed that the presence of impurity atoms in the real CP-Ti crystallite, as well as the strong crystal lattice curvature could facilitate the transformation of local bcc regions into the ω and α″ nanocrystalline phases (with the hexagonal and orthorhombic lattices).

During the UIT processing, intense surface strains of the CP-Ti sample was accompanied by the strong distortion of the crystal lattice, mainly at the boundaries of the α phase fragments. In the present studies, the χ curvature-torsion of the α phase lattice was estimated by assessing the bending extinction contours in the TEM images using the following expression:

$$\chi = \frac{\frac{360}{2\pi} \times M}{\langle L \rangle}, \quad (4)$$

where M was magnification of the TEM images; $<L>$ was the average contour width. It was found that the χ curvature-torsion of the crystal lattice in the surface layer reached 18 deg/μm under strains by the plastic ploughing mechanism, while χ did not exceed 4 deg/μm in the pronounced shear strain regions (at the depth of 70 μm).

The strong distortion of the α phase crystal lattice, accompanied by a perturbation of the electron density, was the cause of the microstructure and phase transformations in the surface layer of the CP-Ti sample during the UIT processing. The electronic configuration of a Ti atom could be written as [Ar] $3d^2 4s^2$. Accordingly, in the ground state, it had four valence electrons in the 3*d* and 4*s* orbitals. With an increase in the electron gas energy due to the crystal lattice distortion, the 4*s* electrons could be decoupled. As a result, one or both *s* electrons could occupy the valence orbital of the higher 3*d* sublevel. Thus, it was the transition of electrons from the 4*s* orbital to the 3*d* one that caused a change in the method of overlapping electron shells and, respectively, the strain-induced α phase transformations.

A clear manifestation of the role of the electronic subsystem in the development of the phase transformations was the change of the low-temperature hcp titanium phase to the high-temperature bcc one upon heating up to 882 °C. Fractions of the *d*-orbitals in bonds of the hcp and bcc crystals were 0.7 and 0.9, respectively [22]. An increase in the kinetic energy of the electron gas with rising temperature caused the transition of electrons from the *s*-orbital to the *d*-one. It enhanced the proportion of electrons in the *d*-orbital of the bond between titanium ions that was the reason for the change in the degree of the bond orientations and, accordingly, the crystal lattice transformation.

The well-known example of the development of the strain-induced phase transformations in titanium was the α→ω one at high pressures (from 2 up to 12 GPa). In this case, the transformation of the hcp α phase (the unit cell volume was 0.0353 nm^3) into the hexagonal ω one (it was 0.0641 nm^3) under compressive stresses was caused by the convergence of positive titanium ions, which resulted in overlapping of the electron orbitals and a similar increase in the concentration of electrons at the *d*-sublevel. Along with the presence of impurities [23], the environment [24], both loading rate and conditions also affected the pressure level at which the α→ω phase transformation had begun. Thus, the ω phase formation occurred at a pressure of ~9 GPa upon impact loading of titanium samples [23]. However, the α→ω phase transition was observed at 4 GPa in the case of high-pressure torsion [25]. Moreover, the ω phase nanoparticles were found in titanium samples after high-speed channel-angular pressing at 2 GPa [26]. It was shear stresses that had determined the development of the phase transformations at significantly lower pressures, and, therefore, enabled to observe the ω and α″ phases after the UIT processing. Obviously, the presence of translational, and even more so, rotational strain modes had promoted the displacement of atoms in certain directions and had facilitated the formation of various crystal lattices in the α phase.

The presence of clusters with the bcc lattice at the α phase grain boundaries made it possible to suggest that the appearance of the ω and α″ nanocrystalline phases had occurred through the intermediate β phase during the UIT processing. Previously, the predominant precipitation of the ω and α″ phases at the grain boundaries was associated exclusively with an increase in stresses [25].

It should be noted that oxygen, which had penetrated into the surface layer of the CP-Ti sample during the UIT processing [27], suppressed the α→ω transformation [23], but could contribute to a change in the β phase cluster to the ω or α″ one during the UIT processing. This was due to the fact that oxygen could result in raising the total atomic displacements in the β phase clusters because of the static component and, consequently, enhancing the instability of their bcc lattice. In this case, the concentration of oxygen atoms determined the number of atomic displacements and, accordingly, could affect both type (β→ω or β→α″) and intensity of the martensitic transformation. It was shown earlier [28] that the β→ω or β→α″ transitions developed upon strains of titanium β-alloys by drawing to ε = 98%. This depended on the size factor of the atomic radii of alloying elements (δR) and, accordingly, the number of atomic displacements. In the case of low δR values, the β→α″ transformation developed, while the β→ω occurred at high δR levels. In other words, the β phase was transformed into α″ at low numbers of atomic displacements but changed into ω at large ones. Thus, the α→β→ω phase transformation, highly likely, was controlled by the process of segregation of oxygen atoms in the studied CP-Ti sample during the UIT processing.

6. Conclusions

Optical profilometry, atomic force microscopy, and molecular dynamics simulation helped elucidate the patterns of the CP-Ti surface roughing upon the UIT processing. The development of the surface plastic strains by the plastic ploughing mechanism caused the formation of small semicircular pile-ups on the processed plate. The distances between them corresponded to those between the centers of the impact spots. The presence of mi-

croroughnesses on the striker surface facilitated roughing of the semicircular pile-ups due to the formation of numerous protrusions and depressions of various shapes and heights.

It was shown by transmission electron microscopy that plastic strains of the CP-Ti sample surface were localized in the layer less than 100 μm thick. The refinement of the α phase grains, caused by intense dislocation slip and twinning, was characterized by the gradient character. Thus, the α phase submicrocrystalline structure with the grain sizes of less than 200 nm was observed in the uppermost layer. At the depth of 5–10 μm, the α phase grains were found with the average size of 10 μm. Inside them, both the banded microstructure and microtwins with the average transverse size of 100 nm were identified. The mean dimension of the α phase grains was 70 μm at the depth of 50 μm that matched the as-received CP-Ti. In this case, the transverse sizes of the fragments separated by adjacent shear bands increased up to 300 nm. At the depth of 70–100 μm, the microstructure consisted of the equiaxed α phase grains, in which dislocations were identical to the as-received CP-Ti.

In the uppermost surface layer of the CP-Ti sample, the ω and α″ nanocrystalline phases that had been formed under the piled-up materials moved along the striker perimeter. It was found by molecular dynamics simulation that the development of the phase transformations was due to the formation of stacking faults, as well as the bcc phase clusters at the α phase sub-grain boundaries during the UIT processing. It was substantiated that the formation of the ω and α″ phases had occurred through the intermediate β phase under the conditions of the high local curvature of the crystal lattice and had been controlled by the segregation of oxygen atoms.

Author Contributions: Conceptualization, A.P.; software, A.D. and A.N.; investigation, M.K., O.P. and E.S.; writing—original draft preparation, A.P., A.D., M.K.; writing—review and editing, A.P. and A.D. All authors have read and agreed to the published version of the manuscript.

Funding: The work was performed according to the Government research assignment for ISPMS SB RAS, Projects FWRW-2021-0010.

Institutional Review Board Statement: Not applicable.

Informed Consent Statement: Not applicable.

Data Availability Statement: The data presented in this study are available on request from the corresponding author.

Conflicts of Interest: The authors declare no conflict of interest.

References

1. Statnikov, E.S.; Korolkov, O.V.; Vityazev, V.N. Physics and Mechanism of Ultrasonic Impact. *Ultrasonics* **2006**, *44*, e533–e538. [CrossRef]
2. Ye, C.; Telang, A.; Gill, A.S.; Suslov, S.; Idell, Y.; Zweiacker, K.; Wiezorek, J.M.K.; Zhou, Z.; Qian, D.; Mannava, S.R.; et al. Gradient Nanostructure and Residual Stresses Induced by Ultrasonic Nano-Crystal Surface Modification in 304 Austenitic Stainless Steel for High Strength and High Ductility. *Mater. Sci. Eng. A* **2014**, *613*, 274–288. [CrossRef]
3. Wu, B.; Wang, P.; Pyoun, Y.-S.; Zhang, J.; Murakami, R. Effect of Ultrasonic Nanocrystal Surface Modification on the Fatigue Behaviors of Plasma-Nitrided S45C Steel. *Surf. Coat. Technol.* **2012**, *213*, 271–277. [CrossRef]
4. Liao, M.; Chen, W.; Bellinger, N. Effects of Ultrasonic Impact Treatment on Fatigue Behavior of Naturally Exfoliated Aluminum Alloys. *Int. J. Fatigue* **2008**, *30*, 717–726. [CrossRef]
5. Mordyuk, B.N.; Karasevskaya, O.P.; Prokopenko, G.I.; Khripta, N.I. Ultrafine-Grained Textured Surface Layer on Zr–1%Nb Alloy Produced by Ultrasonic Impact Peening for Enhanced Corrosion Resistance. *Surf. Coat. Technol.* **2012**, *210*, 54–61. [CrossRef]
6. Mordyuk, B.N.; Prokopenko, G.I. Ultrasonic Impact Peening for the Surface Properties' Management. *J. Sound Vib.* **2007**, *308*, 855–866. [CrossRef]
7. Dekhtyar, A.I.; Mordyuk, B.N.; Savvakin, D.G.; Bondarchuk, V.I.; Moiseeva, I.V.; Khripta, N.I. Enhanced Fatigue Behavior of Powder Metallurgy Ti–6Al–4V Alloy by Applying Ultrasonic Impact Treatment. *Mater. Sci. Eng. A* **2015**, *641*, 348–359. [CrossRef]
8. Panin, A.V.; Kazachenok, M.S.; Kozelskaya, A.I.; Hairullin, R.R.; Sinyakova, E.A. Mechanisms of Surface Roughening of Commercial Purity Titanium during Ultrasonic Impact Treatment. *Mater. Sci. Eng. A* **2015**, *647*, 43–50. [CrossRef]
9. Prigogine, I. *Non-Equilibrium Statistical Mechanics*; Monographs in Statistical Physics and Thermodynamics; Interscience Publisher: New York, NY, USA, 1962; ISBN 978-0-470-69993-5.

10. Chausov, M.; Maruschak, P.; Pylypenko, A.; Markashova, L. Enhancing Plasticity of High-Strength Titanium Alloys VT 22 under Impact-Oscillatory Loading. *Philos. Mag.* **2017**, *97*, 389–399. [CrossRef]
11. Panin, V.E.; Egorushkin, V.E. Basic Physical Mesomechanics of Plastic Deformation and Fracture of Solids as Hierarchically Organized Nonlinear Systems. *Phys. Mesomech.* **2015**, *18*, 377–390. [CrossRef]
12. Panin, V.E.; Panin, A.V.; Perevalova, O.B.; Shugurov, A.R. Mesoscopic Structural States at the Nanoscale in Surface Layers of Titanium and Its Alloy Ti-6Al-4V in Ultrasonic and Electron Beam Treatment. *Phys. Mesomech.* **2019**, *22*, 345–354. [CrossRef]
13. Shugurov, A.R.; Panin, A.V.; Dmitriev, A.I.; Nikonov, A.Y. Recovery of Scratch Grooves in Ti-6Al-4V Alloy Caused by Reversible Phase Transformations. *Metals* **2020**, *10*, 1332. [CrossRef]
14. Plimpton, S. Fast Parallel Algorithms for Short-Range Molecular Dynamics. *J. Comput. Phys.* **1995**, *117*, 1–19. [CrossRef]
15. Dmitriev, A.I.; Nikonov, A.Y.; Shugurov, A.R.; Panin, A.V. The Role of Grain Boundaries in Rotational Deformation in Polycrystalline Titanium under Scratch Testing. *Phys. Mesomech.* **2019**, *22*, 365–374. [CrossRef]
16. Mendelev, M.I.; Underwood, T.L.; Ackland, G.J. Development of an Interatomic Potential for the Simulation of Defects, Plasticity, and Phase Transformations in Titanium. *J. Chem. Phys.* **2016**, *145*, 154102. [CrossRef]
17. Stukowski, A.; Bulatov, V.V.; Arsenlis, A. Automated Identification and Indexing of Dislocations in Crystal Interfaces. *Model. Simul. Mater. Sci. Eng.* **2012**, *20*, 085007. [CrossRef]
18. Panin, A.V.; Kazachenok, M.S.; Kozelskaya, A.I.; Balokhonov, R.R.; Romanova, V.A.; Perevalova, O.B.; Pochivalov, Y.I. The Effect of Ultrasonic Impact Treatment on the Deformation Behavior of Commercially Pure Titanium under Uniaxial Tension. *Mater. Des.* **2017**, *117*, 371–381. [CrossRef]
19. Johnson, K.L. *Contact Mechanics*, 1st ed.; Cambridge University Press: Cambridge, UK, 1985; ISBN 978-0-521-25576-9.
20. Lytvynenko, I.V.; Maruschak, P.O. Analysis of the State of the Modified Nanotitanium Surface with the Use of the Mathematical Model of a Cyclic Random Process. *Optoelectron. Instrum. Process.* **2015**, *51*, 254–263. [CrossRef]
21. Pei, Z. An Overview of Modeling the Stacking Faults in Lightweight and High-Entropy Alloys: Theory and Application. *Mater. Sci. Eng. A* **2018**, *737*, 132–150. [CrossRef]
22. Altmann, S.L.; Coulson, C.A.; Hume-Rothery, W. On the Relation between Bond Hybrids and the Metallic Structures. *Proc. R. Soc. Lond. Ser. A Math. Phys. Sci.* **1957**, *240*, 145–159. [CrossRef]
23. Hennig, R.G.; Trinkle, D.R.; Bouchet, J.; Srinivasan, S.G.; Albers, R.C.; Wilkins, J.W. Impurities Block the α to ω Martensitic Transformation in Titanium. *Nat. Mater.* **2005**, *4*, 129–133. [CrossRef] [PubMed]
24. Errandonea, D.; Meng, Y.; Somayazulu, M.; Häusermann, D. Pressure-Induced Transition in Titanium Metal: A Systematic Study of the Effects of Uniaxial Stress. *Phys. B Condens. Matter* **2005**, *355*, 116–125. [CrossRef]
25. Zhilyaev, A.P.; Popov, V.A.; Sharafutdinov, A.R.; Danilenko, V.N. Shear Induced ω-Phase in Titanium. *LoM* **2011**, *1*, 203–207. [CrossRef]
26. Zel'dovich, V.I.; Frolova, N.Y.; Patselov, A.M.; Gundyrev, V.M.; Kheifets, A.E.; Pilyugin, V.P. The ω-Phase Formation in Titanium upon Deformation under Pressure. *Phys. Met. Metallogr.* **2010**, *109*, 30–38. [CrossRef]
27. Perevalova, O.B.; Panin, A.V.; Kazachenok, M.S. Concentration-Dependent Transformation Plasticity Effect during Hydrogenation of Technically Pure Titanium Irradiated with an Electron Beam. *Russ. Phys. J.* **2019**, *61*, 1992–2000. [CrossRef]
28. Skiba, I.A.; Karasevska, O.I.; Mordyuk, B.N.; Markovsky, P.E.; Shyvaniuk, V.N. Effect of Strain-Induced B→ω Transformation on Mechanical Behaviour of β-Titanium and β-Zirconium Alloys. *Met. Phys. Adv. Technol.* **2009**, *31*, 1573–1587.